Table 1. Mitochondrial ETC Activities in Muscle

	Subject	cI/CS[a]	cI+III/CS[a]	cII/CS[a]	cII+III/CS[a]	cIII/CS[a]	cIV/CS[a]	CS[b]
Muscle biopsy	S1[c]	36	24	N	34	N	N	64
	S2[c]	6	ND	42	43	10	30	57
	S3	N	N	N	55	N	50	54
	S4	145	N	N	N	222	189	109
	S5	<5	ND	N	30	50	N	65

Abbreviations are as follows: N, value in the control range; ND, not done; cI, complex I; cII, complex II; cIII, complex III; cIV, complex IV; cI+III, coupled activity of complexes I and III; and cII+III, coupled activity of complexes II and III. The analyses were performed in different laboratories, and the reference values are diverse (they usually range between 60% and 140% of the mean control value). The values of ETC complex activities out of the control range (specific to each enzymatic activity and to each laboratory) are reported.
[a]Mean control value (%) of CS-normalized ETC complex activities.
[b]Percentage of mean control value.
[c]Sample from autopsy.

ineffective, and the baby died 4 hr after birth. His blood glucose level was normal, as were renal and hepatic parameters; plasma creatine kinase was moderately elevated (861 U/l; normal value [n.v.] < 400), and blood lactate was extremely high (20.1 mM; n.v. < 2). Analysis of urinary organic acids showed elevated levels of 2-OH glutaric acid, whereas plasma and urinary amino acids were within normal ranges. The autopsy examination revealed left ventricular hypoplasia with septum hypertrophy and a patent ductus arteriosus. No brain examination was performed.

The activities of the ETC complexes in autoptic skeletal-muscle homogenate showed severe defects of both coupled cI+cIII and cII+cIII reactions, normalized to citrate synthase (CS), and a decrease in CS-normalized cI (Table 1). In both liver and cultured fibroblasts, the CS-normalized activities of each of the individual ETC complexes were in the control range. Although the coupled cI+cIII activity cannot be reliably assayed in cultured cells,[12] the coupled cII+cIII activity was clearly decreased in S1 fibroblasts (65% of the control mean).

S2 (II-1, family 2) was born at the 34th week of gestation and was the female first child of non-consanguineous Japanese parents. Her birth weight was 1,120 g (−2.2 SDs). Apgar scores were 7 and 8 at 1 and 5 minutes after birth, respectively. There was no family history of neurological or cardiac disease. The pregnancy was complicated by severe intrauterine growth delay and ultrasound-documented hypertrophic cardiomyopathy. On S2's first day of life, she became apnoeic and was intubated as a result of respiratory failure. She initially displayed moderate lactic acidosis, but soon after her admission to Neonatal Medical Center, her lactic acidosis rapidly worsened (blood lactate = 11.2–18.8 mM; n.v. < 2); her hypertrophic cardiomyopathy evolved into severe heart failure, leading to death at the age of 1 day.

The metabolic profile (urinary and plasmatic amino acids, organic acids, and acylcarnitines) showed no significant findings. A liver autoptic specimen showed a severe deficiency of cI (cI/CS ratio = 2.9%); autoptic skeletal-muscle homogenate also showed a cI deficiency together with less pronounced reductions of other ETC complexes (Table 1).

Sisters S3 (II-1, family 3) and S4 (II-3, family 3) are the first and third, respectively, of three siblings and were born to healthy, non-consanguineous Austrian parents. Their brother (II-2) is a healthy, unaffected boy. S3 and S4 were born prematurely at gestational ages of 32 weeks (birth weight = 1,550 g) and 34 weeks (birth weight = 2,170 g), respectively.

Performed at the 20th week of gestation, prenatal organ screening of S3 revealed a suspected malformation of the cerebellum. A postnatal cranial ultrasound showed cerebellar hypoplasia. After birth, she showed distal arthrogryposis, but no other dysmorphic features. At birth, she suffered from respiratory-distress syndrome, and a few hours later, a severe myoclonic epileptic encephalopathy ensued; blood lactic acid at 36 hr of age was 6.4 mM and rose to 14 mM prior to her death by multiorgan failure on the third day of life. Echocardiography showed a normal heart. Metabolic investigations (amino acids in plasma, acylcarnitine profile, and standard newborn screening) were essentially normal. Analysis of organic acids in urine showed excretion of glycerol and 2-OH-glutarate. In frozen postmortem muscle (obtained within 30 min after death), ETC enzyme activities were slightly decreased (Table 1). An autopsy of the brain revealed severe olivopontocerebellar and thalamic hypoplasia and scattered cavitations in the white matter; the visceral organs appeared normal for the gestational age.

Six years later, prenatal organ screening of the sister, S4, showed cerebellar hypoplasia, suggesting the same disease as in S3. Similar to her sister, S4 suffered from neonatal respiratory distress. No dysmorphic features were present. Echocardiography was normal. A cranial ultrasound confirmed cerebellar hypoplasia. Six hours after birth, epileptic encephalopathy ensued; blood lactic acid was 3.5 mM at 2 hr of age and rose to 9 mM at death on the second day of life. Metabolic investigations showed normal newborn-screening results and a normal acylcarnitine profile. Amino acids in plasma were grossly elevated but showed no specific pattern. Analysis of urinary organic acids showed excretion of a "mitochondrial dysfunctional pattern" with malate, fumarate, and 2-OH-glutarate, as

well as vitamin B6 metabolites and N-acetyl-tyrosine. Analysis of frozen postmortem muscle showed elevated levels of ETC activities (Table 1). In both girls, blood glucose concentration and renal and hepatic parameters were in the normal range.

S5 (II-1, family 4) is an 18-year-old young man and is the only offspring of healthy Italian parents who deny consanguinity and originate from a medium-size town in southern Italy. Pregnancy was normal, and delivery was via cesarean section because of a podalic presentation. He was born at term, and his weight at birth was 4,100 g. Weight and motor development were reportedly normal in his first year of life, but he started to show slowly progressive motor deterioration after the age of 10 months, when he manifested unsteadiness in maintaining acquired sitting position. He achieved the ability to walk with a spastic ataxic gait at 3 years of age but lost ambulation by 6 years of age and has been wheelchair bound since then. At 12 years of age, he started manifesting epileptic seizures in the form of prolonged right-side hemiclonic seizures. MRI showed bilateral increased signal intensity in fluid-attenuated-inversion-recovery and T2-weighted sequences in both occipital-cortical and juxtacortical areas (Figures S1A–S1D). Around the same period, he started to have swallowing difficulties. He was admitted for extensive investigation. Thorough blood tests excluded liver and kidney involvement and did not show lactic acidosis. A specific pattern of organic aciduria was excluded. Electrophysiological examination showed a sensory motor polyneuropathy with slowed conduction velocities. During a 5-year follow-up, he showed a slowly progressive downhill course with recurrent treatment-resistant seizures, worsened swallowing impairment, progressive scoliosis, and cognitive deterioration. A muscle biopsy was performed when he was 12 years old. Spectrophotometric assays of the ETC complexes in muscle homogenate showed virtually undetectable cI/CS ratios and reduced cII+cIII/CS and cIII/CS ratios. The other ETC complex activities were within control limits (Table 1). Since the age of 15 years, he has used a percutaneous-endoscopic-gastronomy tube and has developed severe scoliosis with a Cobb angle of 75°. Control MRI performed when he was 17 years old showed cerebellar atrophy, widening of ventricular brain spaces, and scars from cortical necrotic lesions in both occipital areas (Figures S1E–S1H).

In agreement with the Declaration of Helsinki, informed consent for genetic and biochemical studies was signed by the parents of all subjects, and the ethics committee of the Technische Universität München approved the study.

We performed whole-exome sequencing (WES) to investigate the molecular bases of the mitochondrial disease presentations of S1, S4, and S5, as described previously.[13] Coding DNA sequences were enriched with a SureSelect Human All Exon 50 Mb V4 or V5 Kit (Agilent) and subsequently sequenced on a HiSeq2500 system (Illumina). Read alignment to the human reference assembly (UCSC Genome Browser hg19) was done with the Burrows-Wheeler Aligner (version 0.7.5), and single-nucleotide variants and small insertions and deletions were identified with SAMtools (version 0.1.19). On the basis of the rare disease phenotype and a pattern concordant with autosomal-recessive inheritance, we sought genes carrying rare (minor allele frequency [MAF] < 0.1% in 4,500 control exomes) variants predicted to be compound heterozygous or homozygous. We then prioritized variants in genes coding for proteins with known or predicted mitochondrial localization.[14] This filtering strategy led to the identification of recessive variants in *COQ4*, coding for a mitochondrial protein involved in CoQ_{10} biosynthesis,[10] in all three subjects. In S2, we used the SeqCap EZ Library (version 1.0; Roche NimbleGen). Details on the bioinformatics pipeline and variant filtering have been reported recently.[15] Sequencing statistics are provided in Table S1.

We identified *COQ4* mutations (RefSeq accession number NM_016035.3) in four individuals (Figure 1). In S1, we identified a homozygous missense variant, c.433C>G (p.Arg145Gly). Both parents and a healthy sister are heterozygous carriers, and a healthy brother has two reference alleles. No material was available from the deceased sister. S2 was found to be compound heterozygous for a nonsense variant on the paternal allele and a missense variant on the maternal allele: c.[421C>T];[718C>T], p.[Arg141*];[Arg240Cys]. S4 was found to be compound heterozygous for a missense mutation and an exon 5 in-frame deletion: c.[155T>C];[521_523delCCA], p.[Leu52Ser];[Thr174del]. Both variants were also confirmed in the DNA of S3, whereas the parents are heterozygous for only one variant each (the father carries the missense mutation, and the mother carries the deletion). In S5, we identified a homozygous mutation, c.190C>T (p.Pro64Ser). Both parents are heterozygous for this mutation.

None of the identified variants are present in our exome database, which contains 4,500 samples, or in public SNP databases, including dbSNP, the NHLBI Exome Sequencing Project Exome Variant Server, and the Exome Aggregation Consortium (ExAC) Browser. The only exception is the c.718C>T variant (rs143441644), which is reported to have an extremely low frequency (MAF = 0.00023; 28/12,0330 alleles) in the ExAC Browser. Moreover, all missense changes are predicted to be deleterious by several bioinformatics tools (Table S2).

Because of the identified genetic defects, we tested CoQ_{10} levels in available specimens from the subjects. In a muscle biopsy from S1, we detected a clear reduction of CoQ_{10} (32.9 nmol CoQ_{10}/g protein; n.v. = 101–183; 1.16 nmol CoQ_{10}/CS; n.v. = 1.75–3.46). In fibroblasts from S1, the levels of CoQ_{10} were also lower than CoQ_{10} levels in neonatal control fibroblasts (54% of control mean). In frozen muscle from S3, CoQ_{10} was reduced (13.5 nmol CoQ_{10}/g protein; n.v. = 160–1,200; 0.3 nmol CoQ_{10}/CS; n.v. = 2.7–7); in muscle from S4, CoQ_{10} was profoundly reduced (25.7 nmol CoQ_{10}/g protein; n.v. = 160–1,200; 0.1 nmol CoQ_{10}/CS; n.v. = 2.7–7), whereas in S5 muscle, the amount of CoQ_{10} was slightly decreased

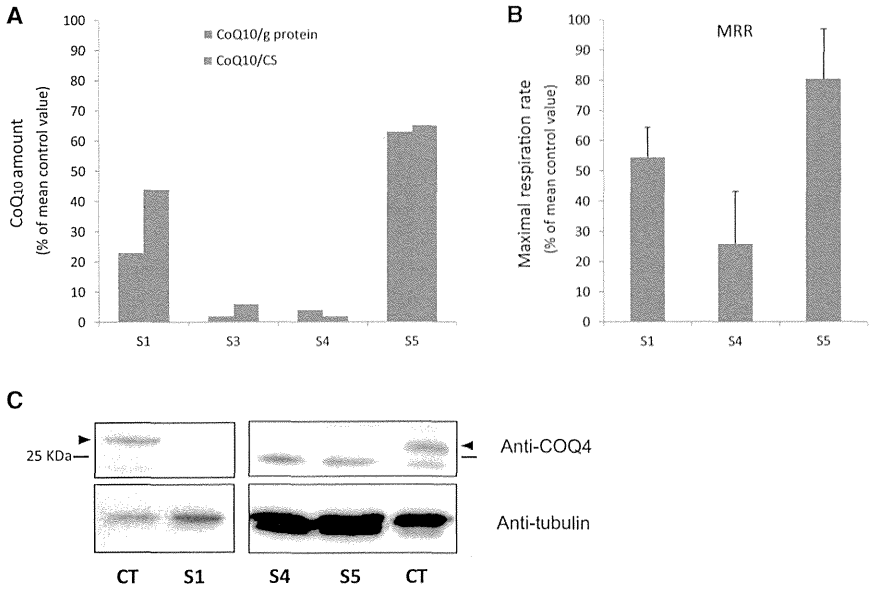

Figure 2. Biochemical Studies in *COQ4* Mutant Muscle and Fibroblasts

(A) CoQ_{10} in muscle from affected subjects S1 and S3–S5 is reported as a percentage of the mean of control values (the analyses were performed in different laboratories, and the reference values are diverse; see text). Data are reported after normalization to protein content or CS activity.

(B) Maximal respiration rate (MRR) measured in fibroblasts from subjects S1, S4, and S5; MRR values are expressed as percentages of MRR values obtained in control fibroblasts. The graphs represent the mean values from two independent experiments, each with six to eight replicates. Error bars represent the SD.

(C) Immunoblot analysis of COQ4 in fibroblasts from subjects S1, S4, and S5 and control individuals (Ct). Arrowheads indicate the band corresponding to COQ4. An antibody against tubulin was used as a loading control.

(88.9 μg CoQ_{10}/g protein; n.v. = 101–183; 1.70 μg nmol CoQ_{10}/CS; n.v. = 1.75–3.46) (Figure 2A). No residual sample from the muscle biopsy of S2 was available. Together, these findings are consistent with a deleterious role of the mutations identified in *COQ4*.

By Seahorse micro-oxygraphy,[16] we detected that maximal respiratory rates were lower in S1, S4, and S5 fibroblasts than in control cells (Figure 2B). Moreover, a drastic decrease in the amount of COQ4 was detected by immunoblot analysis in S1, S4, and S5 fibroblasts (Figure 2C), confirming that the identified *COQ4* nucleotide variants are deleterious.

The *Saccharomyces cerevisiae* ortholog of human *COQ4* is *yCOQ4*; *yCOQ4*-null strains have been reported to be effectively complemented by human *COQ4*.[10] In order to functionally test the effect of all the mutations found in our cohort, we transformed a *COQ4*-null strain (*Δcoq4*) by inserting the following *hCOQ4* variants into the multicopy pYES2.1 vector: pYES:$hCOQ4^{WT}$ (human wild-type [WT]), pYES2.1 (empty vector), pYES:$yCOQ4^{WT}$ (positive control), pYES:hcoq4$^{p.Arg145Gly}$ (mutation c.433C>G), pYES:$hcoq4^{p.Arg141*}$ (c.421C>T), pYES:$hcoq4^{p.Arg240Cys}$ (c.718C>T), pYES:$hcoq4^{p.Leu52Ser}$ (c.155T>C), pYES:$hcoq4^{p.Thr174del}$ (c.521_523delCCA), and pYES:$hcoq4^{p.Pro64Ser}$ (c.190C>T). In addition, to replicate the compound-heterozygous condition found in probands of families 2 and 3, we transformed the *Δcoq4* strain via a pYES construct harboring both the c.155T>C and the c.521_523delCCA mutations (pYES:hcoq4$^{p.Leu52Ser/p.Thr174del}$) and a pYES construct expressing the c.421C>T and c.718C>T mutations (pYES:$hcoq4^{p.Arg141*/p.Arg240Cys}$). A WT strain transformed with the pYES2.1 empty vector was also included as an additional control. In order to reveal a possible respiratory defect, we compared the growth of our transformant strains cultured in either glucose (a fermentable carbon source) or glycerol (a non-fermentable carbon source) after inducing gene expression with galactose for 4 hr. Notably, whereas the growth of the pYES2.1:$hCOQ4^{WT}$ transformant strain was comparable to that of the pYES2.1:$yCOQ4^{WT}$ transformant strain, the strains transformed with the *hCOQ4* mutant vectors grew as slowly as that transformed with pYES2.1 (Figure 3A). This result clearly indicates that each mutation reported in our probands leads to a virtually complete loss of function of the corresponding protein, COQ4. Next, we found that the CoQ_6 content in one *Δcoq4* mutant strain, $hcoq4^{p.Arg145Gly}$, was markedly decreased, whereas *Δcoq4* strains transformed with either pYES2.1:y*COQ4* or pYES2.1:*hCOQ4* had CoQ_6 levels similar to those in the WT strain (Figure 3B). This result indicates that mutant $hcoq4^{p.Arg145Gly}$ impairs CoQ biosynthesis.

Primary CoQ_{10} deficiency, caused by genetic defects in CoQ_{10} biosynthesis, is a clinically heterogeneous condition associated with a spectrum of different phenotypes, including encephalomyopathic forms with seizures and/or ataxia,[17–19] multisystem infantile forms with encephalomyopathy and renal failure,[20] nephrotic syndrome with sensorineural deafness,[21,22] adult Leigh syndrome,[23] and isolated myopathic forms.[24] Mutations in seven genes encoding proteins involved in CoQ_{10} biosynthesis have been reported in single families or in a few singleton cases;[25] the genetic defect has not been determined in most of the cases of CoQ_{10} deficiency, and only a few data are available regarding specific genotype-phenotype correlations. Secondary CoQ_{10} deficiency has been reported in association with glutaric aciduria type IIC (MIM 231680), caused by mutations in *ETFDH* (MIM 231675; encoding electron-transfer dehydrogenase); ataxia-oculomotor apraxia syndrome (MIM 208920), caused by mutations in *APTX* (MIM 606350; encoding aprataxin); a cardiofacio-cutaneous syndrome caused by a mutation in *BRAF* (MIM 115150; encoding serine/threonine-protein kinase B-Raf)[26]; and glucose transporter GLUT1 deficiency.[27]

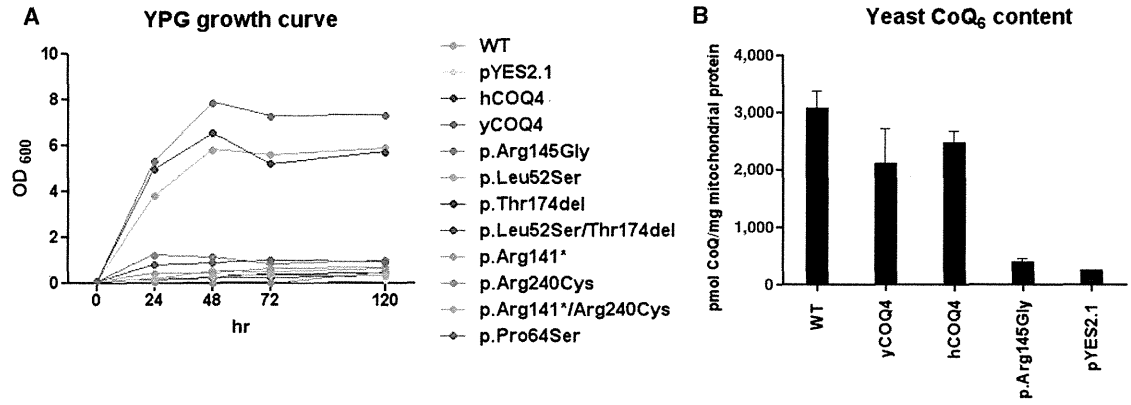

Figure 3. Yeast Studies

(A) Glycerol (YPG) growth of transformed *ΔCOQ4* yeast with the different mutated versions of human *COQ4* (pYES2.1, empty vector; hCOQ4, pYES:*hCOQ4*^{WT}; yCOQ4, pYES:*yCOQ4*^{WT}; c.433C>G, pYES:*hcoq4*$^{p.Arg145Gly}$; c.421C>T, pYES:*hcoq4*$^{p.Arg141*}$; c.718C>T, pYES:*hcoq4*$^{p.Arg240Cys}$; c.155T>C, pYES:*hcoq4*$^{p.Leu52Ser}$; c.521_523delCCA, pYES:*hcoq4*$^{p.Thr174del}$; c.190C>T, pYES:*hcoq4*$^{p.Pro64Ser}$; c.155T>C and c.521_523delCCA, pYES:*hcoq4*$^{p.Leu52Ser/p.Thr174del}$; and c.421C>T and c.718C>T, pYES:*hcoq4*$^{p.Arg141*/p.Arg240Cys}$). WT indicates the wild-type yeast transformed with the YES2.1 empty vector. Cells were grown in selective medium for 16 hr, induced in galactose for 4 hr, and inoculated in YPG at 0.1 U of optical density (OD) at 600 nm. Growth at 30°C was monitored over 5 days by measurement of OD cultures at 600 nm.

(B) Yeast mitochondrial CoQ_6 levels. Purified mitochondria lipid extraction and high-performance-liquid-chromatography quantification of CoQ_6 was performed in the *ΔCOQ4* strain transformed with the empty vector (pYES2.1), WT yeast (yCOQ4), or human (hCOQ4) or *hcoq4*$^{p.Arg145Gly}$ (c.433C>G) *COQ4* genes. A WT strain transformed with the empty vector was included as a positive control. Error bars represent the SD.

Interestingly, although the mechanisms linking these heterogeneous genetic conditions to a decrease in CoQ_{10} remain obscure, most of these individuals benefitted from CoQ_{10} supplementation.[28,29]

We found six *COQ4* mutations in five affected subjects from four unrelated families. All these individuals carried homozygous or compound-heterozygous mutations, clearly indicating that the resulting disease is an autosomal-recessive trait. Two alleles carried nonsense mutations, which are both transmitted by descent in combination with missense *COQ4* mutations to different individuals (S2 and sisters S3 and S4) and are predicted to lead to a truncated and aberrant COQ4. Given that the heterozygous parents carrying the nonsense mutations are alive and well, it is unlikely that COQ4 haploinsufficiency is pathogenic, even though a previous study reported on a boy carrying a de novo heterozygous deletion, including *COQ4*, in chromosomal region 9q34.[30] Because the biosynthetic pathway of CoQ is conserved throughout evolution from human to *Saccharomyces cerevisiae*, we modeled in yeast the mutations found in our subjects. Using this system, we demonstrated that each mutation, or the allelic combinations found in S2 and siblings S3 and S4, was associated with a severe defect of oxidative growth. In parallel, we also showed that COQ4 was strongly reduced in mutant fibroblast cell lines from S1, S4, and S5. In the skeletal muscle of S1 and S3–S5, the CoQ_{10} content was reduced as well. Taken together, these results demonstrate the pathogenic role of the *COQ4* mutations found in our cohort.

In keeping with the essential role of COQ4, four of our five subjects had a prenatal or perinatal onset with a fatal outcome in the first days of life. S1 and S2 presented with severe hypotonia, bradycardia, and respiratory insufficiency at birth; in S2, hypertrophic cardiomyopathy had been evident since fetal development. A markedly different, albeit equally severe, clinical presentation dominated by premature delivery, antenatal cerebellar hypoplasia, neonatal respiratory-distress syndrome, and epileptic encephalopathy characterized sisters S3 and S4. Rapidly progressive, severe lactic acidosis was a common feature in all four affected newborn subjects and is likely to have determined their fatal outcome. Involvement of the heart has been very rarely documented in CoQ_{10}-deficient subjects, often as part of multisystem phenotypes, where cardiomyopathy develops later than brain, muscle, or kidney impairment.[20] For instance, a homozygous nonsense mutation in *COQ9* was described in a baby who presented with neonatal lactic acidosis and later developed hypertrophic cardiomyopathy as part of a multisystem disease including intractable seizures, global developmental delay, and renal tubular dysfunction.[9] In spite of his early onset, the clinical course of S5 was slowly progressive and dominated by neurological deterioration with hardly any involvement of other organs, including the heart and kidneys.

Although the link between specific genetic defects and phenotypes is often unclear in mitochondrial disorders, organs with the highest energy requirements, such as the heart, kidneys, and brain, have the highest CoQ_{10} concentrations[31] and are the most frequently affected by CoQ_{10} deficiency. The level of expression of *COQ* genes in different cells seems to correlate poorly with the primarily affected tissue or organ; for instance, *COQ2*, mutations of which typically cause renal impairment, has expression

levels that are relatively higher in skeletal muscle and the heart than in other organs,[32] whereas *COQ4*, mutated in our subjects with cardiac or brain failure, is ubiquitously expressed and has relatively higher levels in the liver, lungs, and pancreas.

Because cardiomyocytes have a remarkably high energy requirement, and cardiomyopathy is quite common in individuals with various inherited mitochondrial disorders, the cardiac involvement in subjects with mutations in *COQ* genes can be overlooked. Indeed, the crucial role of CoQ_{10} in cardiomyocyte function has been recognized for a very long time; for instance, myocardial biopsies from individuals with congestive heart failure[33] or cardiomyopathy[34,35] show low CoQ_{10} levels, which correlate with the severity of heart damage.[36] Moreover, statins, cholesterol-lowering drugs that inhibit HMG-CoA reductase (the key enzyme common to the biosynthesis of both cholesterol and CoQ_{10}) can cause CoQ_{10} deficiency, ultimately leading to cardiomyopathy;[37] interestingly, this harmful side effect can be overcome by oral CoQ_{10} supplementation.[38] Moreover, long-term CoQ_{10} treatment of individuals with chronic heart failure is safe, improves symptoms, and reduces major adverse cardiovascular events.[39] These observations all converge on a strict association between CoQ_{10} deficiency and cardiomyopathy.

Notably, S3–S5 showed no sign of heart involvement, whereas the clinical phenotype was dominated by encephalopathy with seizures and a more progressive, but mainly neurological, syndrome is the clinical hallmark of S5, indicating the heterogeneity of the clinical presentations associated with *COQ4* defects. The variable specificity of organ failure (e.g., heart versus brain) in the neonatal cases of our cohort could be due to the fulminant course of the disease, which prevented the deployment of multisystem involvement. In support of this view, although cardiomyopathy dominated the clinical picture, the presence of severe hypotonia and hyporeflexia suggests concomitant involvement of the nervous system in S1 and S2 as well. Clinical heterogeneity was accompanied by an equally striking variability of the biochemical findings, which ranged from multiple (S1 and S5) to isolated (S2 and S3) ETC defects in muscle and fibroblasts to hardly any detectable defect at all (S4). This biochemical diversity could be due to differences in individual adaptive responses to reduced CoQ_{10} availability or could reflect the striking tissue specificity observed in the clinical presentations, but at the moment, a mechanistic explanation for these observations is lacking. Poor correlation with the clinical and biochemical phenotypes has also been reported for other genes related to CoQ_{10} biosynthesis. For instance, mutations in *COQ2*, the first mutated gene identified in affected individuals with primary CoQ_{10} deficiency, have been associated with a wide range of clinical presentations, often including nephrotic syndrome but also including fatal neonatal multisystemic disorder, Leigh syndrome, myoclonic epilepsy, hypertrophic cardiomyopathy, deafness, and adult-onset multisystem atrophy.[25,40] In any case, the identification of *COQ4* mutations in subjects with such a wide spectrum of clinical and biochemical abnormalities is a further indication of the advantage of unbiased screening such as WES for the identification of genes newly associated with mitochondrial disorders.

Unfortunately, the fulminant fatal outcome in S1–S4 was so rapid that it prevented both the diagnosis of CoQ_{10} deficiency and the start of CoQ_{10} supplementation. Prompt diagnosis is a main challenge for syndromes of primary CoQ10 deficiency but is very important given that co-factor deficiencies are virtually the only group of mitochondrial disorders for which beneficial pharmacological treatment is currently available. Treatment of the long-surviving subject, S5, has now started and will hopefully provide some useful indication of its efficacy in the near future.

Supplemental Data

Supplemental Data include one figure and two tables and can be found with this article online at http://dx.doi.org/10.1016/j.ajhg.2014.12.023.

Acknowledgments

We would like to thank the families for their collaboration. We thank Roberto Bellavia, Yoshihito Kishita, Yoshimi Tokuzawa, and Ana Sánchez-Cuesta for their technical support; Consolato Sergi for his help; and K. Muroya and M. Adachi for referral of subject materials. This work was supported by Fondazione Telethon (GGP11011), the Italian Ministry of Health (GR2010–2316392 [D.G.]; "Ricerca corrente" [E.B.]), Fondazione CARIPLO (2011/0526), the Mariani Foundation, the Italian Association of Mitochondrial Disease Patients and Families (Mitocon), the European Research Council Advanced Grant FP7-322424, the German Ministry of Education and Research through the E-Rare project GENOMIT (01GM1207 [T.M.; H.P.], FWF I 920-B13 [J.A.M.], J41J11000420001 [D.G.]), the German Network for mitochondrial disorders (mitoNET; 01GM1113C [T.M.; H.P.]), the German Center for Heart Research (Z76010017300; Z56010015300 [T.M.]) by the German Research Foundation within the Munich Cluster for Systems Neurology (EXC-1010-SyNergy), the UK Medical Research Council, the Spanish Instituto de Salud Carlos III (FIS-PI11-00078), the Research Program of Innovative Cell Biology by Innovative Technology (Cell Innovation) from the Japanese Ministry of Education, Culture, Sports, Science, and Technology [Y.O.], Grants-in-Aid for the Research on Intractable Diseases (Mitochondrial Disease) from the Ministry of Health, Labour, and Welfare of Japan [A.O.; K.M.], and the Kawano Masanori Memorial Public Interest Incorporated Foundation for Promotion of Pediatrics [K.M.]. We also acknowledge the Cell Lines and DNA Bank of Paediatric Movement Disorders and Mitochondrial Diseases and the Bank of Muscle Tissue, Peripheral Nerve, DNA, and Cell Culture of the Telethon Network of Genetic Biobanks (grant GTB12001J) and the EurobiobanK Network.

Received: November 20, 2014
Accepted: December 18, 2014
Published: February 5, 2015

Web Resources

The URLs for data presented herein are as follows:

Exome Aggregation Consortium (ExAC) Browser, http://exac.broadinstitute.org/

NHLBI Exome Sequencing Project (ESP) Exome Variant Server, http://evs.gs.washington.edu/EVS/

OMIM, http://www.omim.org

UCSC Genome Browser, http://genome.ucsc.edu

References

1. Turunen, M., Olsson, J., and Dallner, G. (2004). Metabolism and function of coenzyme Q. Biochim. Biophys. Acta *1660*, 171–199.
2. Echtay, K.S., Winkler, E., and Klingenberg, M. (2000). Coenzyme Q is an obligatory cofactor for uncoupling protein function. Nature *408*, 609–613.
3. Miller, R.W., and Curry, J.R. (1969). Mammalian dihydroorotate—ubiquinone reducatse complex. II. Correlation with cytochrome oxidase, mode of linkage with the cytochrome chain, and general properties. Can. J. Biochem. *47*, 725–734.
4. Schmelzer, C., Lorenz, G., Rimbach, G., and Döring, F. (2007). Influence of Coenzyme Q_10 on release of pro-inflammatory chemokines in the human monocytic cell line THP-1. Biofactors *31*, 211–217.
5. Bentinger, M., Tekle, M., and Dallner, G. (2010). Coenzyme Q—biosynthesis and functions. Biochem. Biophys. Res. Commun. *396*, 74–79.
6. Kawamukai, M. (2009). Biosynthesis and bioproduction of coenzyme Q10 by yeasts and other organisms. Biotechnol. Appl. Biochem. *53*, 217–226.
7. Quinzii, C.M., Emmanuele, V., and Hirano, M. (2014). Clinical presentations of coenzyme q10 deficiency syndrome. Mol Syndromol *5*, 141–146.
8. Zeviani, M., and Carelli, V. (2007). Mitochondrial disorders. Curr. Opin. Neurol. *20*, 564–571.
9. Duncan, A.J., Bitner-Glindzicz, M., Meunier, B., Costello, H., Hargreaves, I.P., López, L.C., Hirano, M., Quinzii, C.M., Sadowski, M.I., Hardy, J., et al. (2009). A nonsense mutation in COQ9 causes autosomal-recessive neonatal-onset primary coenzyme Q10 deficiency: a potentially treatable form of mitochondrial disease. Am. J. Hum. Genet. *84*, 558–566.
10. Casarin, A., Jimenez-Ortega, J.C., Trevisson, E., Pertegato, V., Doimo, M., Ferrero-Gomez, M.L., Abbadi, S., Artuch, R., Quinzii, C., Hirano, M., et al. (2008). Functional characterization of human COQ4, a gene required for Coenzyme Q10 biosynthesis. Biochem. Biophys. Res. Commun. *372*, 35–39.
11. Marbois, B., Gin, P., Gulmezian, M., and Clarke, C.F. (2009). The yeast Coq4 polypeptide organizes a mitochondrial protein complex essential for coenzyme Q biosynthesis. Biochim. Biophys. Acta *1791*, 69–75.
12. Spinazzi, M., Casarin, A., Pertegato, V., Salviati, L., and Angelini, C. (2012). Assessment of mitochondrial respiratory chain enzymatic activities on tissues and cultured cells. Nat. Protoc. *7*, 1235–1246.
13. Haack, T.B., Haberberger, B., Frisch, E.M., Wieland, T., Iuso, A., Gorza, M., Strecker, V., Graf, E., Mayr, J.A., Herberg, U., et al. (2012). Molecular diagnosis in mitochondrial complex I deficiency using exome sequencing. J. Med. Genet. *49*, 277–283.
14. Elstner, M., Andreoli, C., Klopstock, T., Meitinger, T., and Prokisch, H. (2009). The mitochondrial proteome database: MitoP2. Methods Enzymol. *457*, 3–20.
15. Ohtake, A., Murayama, K., Mori, M., Harashima, H., Yamazaki, T., Tamaru, S., Yamashita, Y., Kishita, Y., Nakachi, Y., Kohda, M., et al. (2014). Diagnosis and molecular basis of mitochondrial respiratory chain disorders: exome sequencing for disease gene identification. Biochim. Biophys. Acta *1840*, 1355–1359.
16. Invernizzi, F., D'Amato, I., Jensen, P.B., Ravaglia, S., Zeviani, M., and Tiranti, V. (2012). Microscale oxygraphy reveals OXPHOS impairment in MRC mutant cells. Mitochondrion *12*, 328–335.
17. Ogasahara, S., Engel, A.G., Frens, D., and Mack, D. (1989). Muscle coenzyme Q deficiency in familial mitochondrial encephalomyopathy. Proc. Natl. Acad. Sci. USA *86*, 2379–2382.
18. Lamperti, C., Naini, A., Hirano, M., De Vivo, D.C., Bertini, E., Servidei, S., Valeriani, M., Lynch, D., Banwell, B., Berg, M., et al. (2003). Cerebellar ataxia and coenzyme Q10 deficiency. Neurology *60*, 1206–1208.
19. Mignot, C., Apartis, E., Durr, A., Marques Lourenço, C., Charles, P., Devos, D., Moreau, C., de Lonlay, P., Drouot, N., Burglen, L., et al. (2013). Phenotypic variability in ARCA2 and identification of a core ataxic phenotype with slow progression. Orphanet J. Rare Dis. *8*, 173.
20. Rötig, A., Appelkvist, E.-L., Geromel, V., Chretien, D., Kadhom, N., Edery, P., Lebideau, M., Dallner, G., Munnich, A., Ernster, L., and Rustin, P. (2000). Quinone-responsive multiple respiratory-chain dysfunction due to widespread coenzyme Q10 deficiency. Lancet *356*, 391–395.
21. Heeringa, S.F., Chernin, G., Chaki, M., Zhou, W., Sloan, A.J., Ji, Z., Xie, L.X., Salviati, L., Hurd, T.W., Vega-Warner, V., et al. (2011). COQ6 mutations in human patients produce nephrotic syndrome with sensorineural deafness. J. Clin. Invest. *121*, 2013–2024.
22. Ashraf, S., Gee, H.Y., Woerner, S., Xie, L.X., Vega-Warner, V., Lovric, S., Fang, H., Song, X., Cattran, D.C., Avila-Casado, C., et al. (2013). ADCK4 mutations promote steroid-resistant nephrotic syndrome through CoQ10 biosynthesis disruption. J. Clin. Invest. *123*, 5179–5189.
23. Van Maldergem, L., Trijbels, F., DiMauro, S., Sindelar, P.J., Musumeci, O., Janssen, A., Delberghe, X., Martin, J.J., and Gillerot, Y. (2002). Coenzyme Q-responsive Leigh's encephalopathy in two sisters. Ann. Neurol. *52*, 750–754.
24. Lalani, S.R., Vladutiu, G.D., Plunkett, K., Lotze, T.E., Adesina, A.M., and Scaglia, F. (2005). Isolated mitochondrial myopathy associated with muscle coenzyme Q10 deficiency. Arch. Neurol. *62*, 317–320.
25. Doimo, M., Desbats, M.A., Cerqua, C., Cassina, M., Trevisson, E., and Salviati, L. (2014). Genetics of coenzyme q10 deficiency. Mol Syndromol *5*, 156–162.
26. Aeby, A., Sznajer, Y., Cavé, H., Rebuffat, E., Van Coster, R., Rigal, O., and Van Bogaert, P. (2007). Cardiofaciocutaneous (CFC) syndrome associated with muscular coenzyme Q10 deficiency. J. Inherit. Metab. Dis. *30*, 827.
27. Yubero, D., O Callaghan, M., Montero, R., Ormazabal, A., Armstrong, J., Espinos, C., Rodríguez, M.A., Jou, C., Castejon, E., Aracil, M.A., et al. (2014). Association between coenzyme Q 10 and glucose transporter (GLUT1) deficiency. BMC Pediatr. *14*, 284.
28. Musumeci, O., Naini, A., Slonim, A.E., Skavin, N., Hadjigeorgiou, G.L., Krawiecki, N., Weissman, B.M., Tsao, C.Y., Mendell,

J.R., Shanske, S., et al. (2001). Familial cerebellar ataxia with muscle coenzyme Q10 deficiency. Neurology *56*, 849–855.
29. DiMauro, S., Schon, E.A., Carelli, V., and Hirano, M. (2013). The clinical maze of mitochondrial neurology. Nat Rev Neurol *9*, 429–444.
30. Salviati, L., Trevisson, E., Rodriguez Hernandez, M.A., Casarin, A., Pertegato, V., Doimo, M., Cassina, M., Agosto, C., Desbats, M.A., Sartori, G., et al. (2012). Haploinsufficiency of COQ4 causes coenzyme Q10 deficiency. J. Med. Genet. *49*, 187–191.
31. Aberg, F., Appelkvist, E.L., Dallner, G., and Ernster, L. (1992). Distribution and redox state of ubiquinones in rat and human tissues. Arch. Biochem. Biophys. *295*, 230–234.
32. Forsgren, M., Attersand, A., Lake, S., Grünler, J., Swiezewska, E., Dallner, G., and Climent, I. (2004). Isolation and functional expression of human COQ2, a gene encoding a polyprenyl transferase involved in the synthesis of CoQ. Biochem. J. *382*, 519–526.
33. Hanaki, Y., Sugiyama, S., Ozawa, T., and Ohno, M. (1991). Ratio of low-density lipoprotein cholesterol to ubiquinone as a coronary risk factor. N. Engl. J. Med. *325*, 814–815.
34. Langsjoen, P.H., Langsjoen, P.H., and Folkers, K. (1990). Long-term efficacy and safety of coenzyme Q10 therapy for idiopathic dilated cardiomyopathy. Am. J. Cardiol. *65*, 521–523.
35. Manzoli, U., Rossi, E., Littarru, G.P., Frustaci, A., Lippa, S., Oradei, A., and Aureli, V. (1990). Coenzyme Q10 in dilated cardiomyopathy. Int. J. Tissue React. *12*, 173–178.
36. Mortensen, S.A., Vadhanavikit, S., and Folkers, K. (1984). Deficiency of coenzyme Q10 in myocardial failure. Drugs Exp. Clin. Res. *10*, 497–502.
37. Silver, M.A., Langsjoen, P.H., Szabo, S., Patil, H., and Zelinger, A. (2003). Statin cardiomyopathy? A potential role for Co-Enzyme Q10 therapy for statin-induced changes in diastolic LV performance: description of a clinical protocol. Biofactors *18*, 125–127.
38. Ghirlanda, G., Oradei, A., Manto, A., Lippa, S., Uccioli, L., Caputo, S., Greco, A.V., and Littarru, G.P. (1993). Evidence of plasma CoQ10-lowering effect by HMG-CoA reductase inhibitors: a double-blind, placebo-controlled study. J. Clin. Pharmacol. *33*, 226–229.
39. Mortensen, S.A., Rosenfeldt, F., Kumar, A., Dolliner, P., Filipiak, K.J., Pella, D., Alehagen, U., Steurer, G., and Littarru, G.P.; Q-SYMBIO Study Investigators (2014). The effect of coenzyme Q10 on morbidity and mortality in chronic heart failure: results from Q-SYMBIO: a randomized double-blind trial. JACC Heart Fail *2*, 641–649.
40. Scalais, E., Chafai, R., Van Coster, R., Bindl, L., Nuttin, C., Panagiotaraki, C., Seneca, S., Lissens, W., Ribes, A., Geers, C., et al. (2013). Early myoclonic epilepsy, hypertrophic cardiomyopathy and subsequently a nephrotic syndrome in a patient with CoQ_{10} deficiency caused by mutations in para-hydroxybenzoate-polyprenyl transferase (COQ2). Eur. J. Paediatr. Neurol. *17*, 625–630.

The American Journal of Human Genetics
Supplemental Data

COQ4 Mutations Cause a Broad Spectrum of Mitochondrial Disorders Associated with CoQ_{10} Deficiency

Gloria Brea-Calvo, Tobias B. Haack, Daniela Karall, Akira Ohtake, Federica Invernizzi, Rosalba Carrozzo, Laura Kremer, Sabrina Dusi, Christine Fauth, Sabine Scholl-Bürgi, Elisabeth Graf, Uwe Ahting, Nicoletta Resta, Nicola Laforgia, Daniela Verrigni, Yasushi Okazaki, Masakazu Kohda, Diego Martinelli, Peter Freisinger, Tim M. Strom, Thomas Meitinger, Costanza Lamperti, Atilano Lacson, Placido Navas, Johannes A. Mayr, Enrico Bertini Kei Murayama, Massimo Zeviani, Holger Prokisch, and Daniele Ghezzi

SUPPLEMENTAL DATA

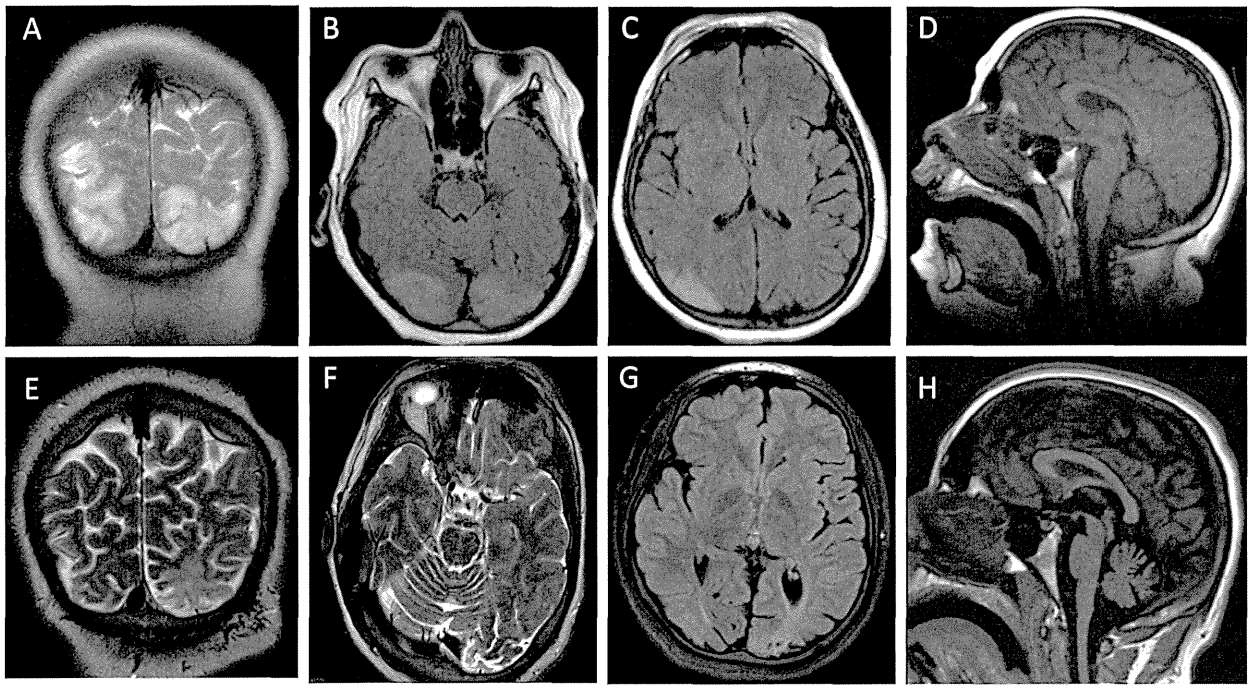

Figure S1. Brain MRI of subject 5.

Two serial brain MRI images of subject S5 obtained at age 12 years (A-D) and at age 17 years (E-H). A and E are coronal T2 weighted sections to show abnormal hyperintense cortical areas corresponding to infarct-like lesions of the occipital lobes at two different stages of progression to cortical atrophy with scars (E-G); The same occipital abnormal hyperintense cortical areas are shown in axial sections B and C (FLAIR weighted), F (T2 weighted) and G (FLAIR weighted). Notice that no abnormality is present in basal ganglia and brainstem. Finally, figures D and H are sagittal T1 sections showing progressive cerebellar atrophy of the vermis.

Id	Type	Reads	Mapped	Percent	Seq (Gb)	on bait	Avg cov	Cov 1x	Cov 4x	Cov 8x	Cov 20x
S1	SureSelect50Mbv5	106627996	105933934	99.35	10.77	78.48	132.44	99.92	99.72	99.35	97.38
S2	SeqCapEZ V1	130889538	125611825	95.97	13.81	62.71	155.83	98.36	97.32	96.41	93.80
S4	SureSelect50Mbv5	90821087	90214603	99.33	9.17	78.99	113.62	99.80	99.52	99.05	96.55
S5	SureSelect50Mbv4	125822167	124979728	99.33	12.71	73.98	146.50	99.95	99.80	99.55	98.22

Table S1: Exome Sequencing Statistics

Avg: average; Cov: coverage

Nucleotide Change	Amino acid Change	Subject	Status	Polyphen2	SIFT	PMUT	Mutation taster
c.[433C>G]	p.[Arg145Gly]	S1	Homozygous	Probably damaging	Deleterious	Pathological	Disease causing
c.[718C>T]	p.[Arg240Cys]	S2	CE with a nonsense mutation p.[Arg141*]	Probably damaging	Deleterious	Pathological	Disease causing
c.[155T>C]	p.[Leu52Ser]	S3, S4	CE with a deletion p.[Thr174del]	Probably damaging	Deleterious	Neutral	Disease causing
c.[190C>T]	p.[Pro64Ser]	S5	Homozygous	Probably damaging	Deleterious	Neutral	Disease causing

Table S2: In silico prediction of pathogenicity for *COQ4* mutations

CE: compound heterozygous.

PLOS ONE

Evolution of Mitochondrial Power in Vertebrate Metazoans

Yasuhiro Kitazoe[1]*, Masashi Tanaka[2]

1 Center of Medical Information Science, Kochi Medical School, Nankoku, Kochi, Japan, **2** Department of Genomics for Longevity and Health, Tokyo Metropolitan Institute of Gerontology, Tokyo, Japan

Abstract

Background: Basal metabolic rate (*BMR*) has a very strong body-mass (*M*) dependence in an individual animal group, and *BMR* per unit mass (*msBMR*) converges on a markedly narrow range even across major taxonomic groups. However, it is here a basic question in metazoan biology how much *BMR* per unit mitochondrion (*mtBMR*) changes, and then whether *mtBMR* can be related to the original molecular mechanism of action of mt-encoded membrane proteins (MMPs) playing a central role in cellular energy production.

Methodology/Principal Findings: Analyzing variations of amino-acid compositions of MMPs across 13 metazoan animal groups, incorporating 2022 sequences, we found a strong inverse correlation between Ser/Thr composition (*STC*) and hydrophobicity (*HYD*). A majority of animal groups showed an evolutionary pathway of a gradual increase in *HYD* and decrease in *STC*, whereas only the deuterostome lineage revealed a rapid decrease in *HYD* and increase in *STC*. The strongest correlations appeared in 5 large subunits (ND4, ND5, ND2, CO1, and CO3) undergoing dynamic conformational changes for the proton-pumping function. The pathway of the majority groups is well understood as reflecting natural selection to reduce *mtBMR*, since simply raising *HYD* in MMPs (surrounded by the lipid bilayer) weakens their mobility and strengthens their stability. On the other hand, the marked decrease in *HYD* of the deuterostome elevates *mtBMR*, but is accompanied with their instability heightening a turnover rate of mitochondria and then cells. Interestingly, cooperative networks of interhelical hydrogen-bonds between motifs involving Ser and Thr residues can enhance MMP stability.

Conclusion/Significance: This stability enhancement lowers turnover rates of mitochondria/cells and may prolong even longevity, and was indeed founded by strong positive correlations of *STC* with both *mtBMR* and longevity. The lowest *HYD* and highest *STC* in Aves and Mammals are congruent with their very high *mtBMR* and long longevity.

Citation: Kitazoe Y, Tanaka M (2014) Evolution of Mitochondrial Power in Vertebrate Metazoans. PLoS ONE 9(6): e98188. doi:10.1371/journal.pone.0098188

Editor: Yidong Bai, University of Texas Health Science Center at San Antonio, United States of America

Received March 11, 2014; **Accepted** April 25, 2014; **Published** June 9, 2014

Data Availability: The authors confirm that all data underlying the findings are fully available without restriction. All data are in the manuscript and accession numbers of amino acid sequences are in the supplemental file S1.

Funding: This work was supported by Grants-in-Aid for Scientific Research from the Ministry of Education, Culture, Sports, Science, and Technology of Japan (A-22240072 B-21390459 and C-21590411 to M.T.) by Grants-in-Aid for Research on Intractable Diseases (Mitochondrial Disorders) from the Ministry of Health, Labor, and Welfare of Japan (23-016, 23-116 and 24-005 to M.T.) and by grants for scientific research from the Takeda Science Foundation (to M.T.). The funders had no role in study design, data collection and analysis, decision to publish, or preparation of the manuscript.

Competing Interests: The authors have declared that no competing interests exist.

* E-mail: kitazoeyasuhiro@yahoo.co.jp

Introduction

Because the basal metabolic rate (*BMR*) is a fundamental currency to sustain metazoan life, it must be profoundly relevant to the mt power in energy production. However, its strong mass (*M*)-dependence makes unclear the existence of a relationship between *BMR* and this mitochondrial (mt) energy power across major taxonomic groups. A recent allometric study reports that the mass specific BMT (*msBMR*) converges on a markedly narrow range in these groups [1]. This viewpoint of the normalized energy inclines us to convert *msBMR* into the mt *BMR* (*mtBMR*) per unit mitochondrion which stands for the mt energy power, since the conversion can be done when *msBMR* includes the falling effect of the mt density (the mean number of mitochondria per unit cell) with increasing *M* [2], [3]. It is intriguing to estimate how much *mtBMR* changes across taxonomic groups, because recent structural studies report a high degree of sequence conservation of the membrane integral central subunits [4], [5], the mechanism of which is therefore likely to be similar throughout species [6].

The first step to relate *mtBMR* to the mt energy production power is to investigate the molecular structure of mt-encoded membrane proteins (MMPs) by using a number of amino acid sequences which are available in the NCBI database [7] (the accession numbers of these sequences are listed up in Table S1). The great majority of MMPs belongs to the 3 proton-pumping complexes of I, III and IV. Recent structural studies suggest that proton translocation in complex I requires large dynamic conformational changes across several subunits [6], [8], [9]. Likewise, the two large subunits of complex IV, i.e., CO1 and CO3, transfer protons across the membrane via conformational changes induced by electron transport [10–12].

MMPs are mostly embedded in the hydrophobic environment of the lipid bilayer, and their amino acid composition is primarily hydrophobic, with approximately 90–95% of these amino acids

being non-polar. Therefore, the degree (mobility) of their conformational changes much depends on hydrophobicity (*HYD*): Raising *HYD* weakens their mobility and strengthens their stability according to the trade-off relation between mobility and stability [13]. Interestingly, a recent study of membrane proteins reports that the dynamic conformational stability of membrane helices can be typically enhanced by cooperative networks of interhelical hydrogen bonds between moderately polar residues, notably Ser and Thr [13–15]. The above-mentioned two features of *HYD* and Ser/Thr composition (*STC*) allow us to conceive a basic scenario of the metazoan evolution that lowering *mtBMR* (on the basis of the multicellular effect) requires less dynamic conformational changes of MMPs which induce an increase in *HYD* and a decrease in *STC*.

Here we report that most members of major animal groups follow this evolutionary scenario. However, the deuterostome lineage reveals the converse, i.e., rapid increases in *STC* and *mtBMR*, and a rapid decrease in *HYD* toward the endpoints (Aves and Mammals) of this lineage. Aves and Mammals seem ready to power up the mt energy by activating dynamical conformational changes of MMPs and still then enhance stability (durability) of them by increasing helix-helix interactions. This durability lowers turnover rates of mitochondria and cells, and may prolong longevity of organisms. Indeed, a strong correlation between *STC* and maximum lifespan (*MLS*) (observed in a previous vertebrate analysis [16]) was found to extend as a global rule beyond vertebrates across metazoans.

Materials and Methods

Derivation of *mtBMR* from *msBMR*

The allometric scaling law provides a very strong correlation between *BMR* and *M* in each animal group, and is expressed as $BMR = C \cdot M^{\alpha}$ with an allometric exponent α and constant *C*. Makarieva et al. [1] well described a variation of *BMR* data across different animal groups by using *BMR* per unit mass (*msBMR*), i.e., $msBMR = C \cdot M^{-(1-\alpha)}$

They reported that *msBMR* data across dramatically different life forms converge on a markedly narrow range. This unit-mass representation of *msBMR* implicitly means that an organism is approximately regarded as a homogeneous matter of standard (representative) cells: the number of cells in unit mass and also that of mitochondria (the mt density) in unit cell are invariant, respectively, although, in practice, metabolically active cells, such as those of the liver, kidneys, muscles, and brain, have hundreds or thousands of mitochondria [17]. Therefore, *msBMR* is proportional to *BMR* per unit cell (we put this proportional constant equal to 1.0). Next, to get *BMR* per unit mitochondrion, we divide *msBMR* by the factor $M^{-\beta}$ which takes into account the decreasing effect of the mt density with increasing *M* [2], [3]. Then we have $mtBMR = (C/D) \cdot M^{-(1-\alpha-\beta)}$, which means that *mtBMR* decreases with increasing *M* more slowly than does *msBMR*. In this paper, we express *mtBMR* as follows: $mtBMR = C \cdot M^{-(1-\alpha)/F}$. Here, *F* is with a new parameter to adjust the allometric scaling effect of the *M*-dependence. For simplicity, we put the proportional constant *D* equal to 1.0, since the value of $F = 1.0$ corresponds to *msBMR*. In a previous mammalian analysis, the value of $F = 3.0$ was selected as providing the strongest correlation between *mtBMR* and *MLS* [16]. In the present analysis, we redefine *M* as the mean value of the individual body masses in each animal group, to examine a relationship between *mtBMR* and amino acid compositions of MMPs in major taxonomic groups.

Data retrieval

To select a hydrophobic domain in MMPs, we applied the primary structure analysis (ExPASy Proteomics Server; http://www.expasy.ch/), using a standard model for the hydrophobic score (*HYDSC*) given by Cowan and Whittaker [18]. We calculated the moving average, *S*(n), of *HYDSC*(m; m takes n-1, n, and n+1) around the n-th amino acid site in a protein and obtained a smooth function *S*(n) of n by repeating this procedure. As a result, *HYD* was defined as the average value of *S*(n) with $S(n) > 0.0$ in all or selected proteins of a given species. The obtained *HYD* is suitable for examining correlations with other quantities of present interest, such as amino acid compositions and lifespan. We predicted the helix domain of MMPs by using SOSUI and TMHMM servers [19], [20].

Results

A) *HYD-TC* correlation within respective MMPs

By including 13 metazoan animal groups with many amino acid sequences (more than 20) in the NCBI database [7], we analyzed 13 MMPs with a score $S > 0$ for their hydrophobic domain (Materials and Methods). As a result, we selected 4 MMP variables (*HYD*, *STC*, *TC* and *CC*) of amino acid compositions as having significant correlations with one another, and found that *HYD-TC* provided an especially strong correlation. Here, TC and CC denote the Thr and Cys compositions, respectively. Table 1 shows a list of MMPs in the order of strong correlations. The 3 large subunits of ND4, ND5, and ND2 in complex I appeared as the first group with the largest R^2-values ($R^2 > 0.86$). Likewise, 2 large subunits of CO1 and CO3 in complex IV appeared as the second group (with $R^2 > 0.78$). These subunits just correspond to the proteins which require dynamic conformational changes for proton translocation [6], [8], [9]. The *TC-CC* correlation was appreciable in only these 2 proton-pumping complexes (with $R^2 > 0.40$) undergoing dynamic conformational changes in their helices.

B) Correlations between the MMP variables (*HYD, STC, TC* and *CC*)

We investigated the intra-correlations between the MMP variables, by using the following 5 sets of proteins according to the order of strong correlations shown in Table 1: **1**) 3-protein set (ND4, ND5, ND2), **2**) 4-protein set (ND4, ND5, ND2, ND1), **3**) 5-protein set (ND4, ND5, ND2, CO1, CO3), **4**) 6-protein set (ND4, ND5, ND2, CO1, CO3, ND1), and **5**) 7-protein set (ND4, ND5, ND2, CO1, CO3, ND1, CYTB). Here, the 3-protein set included 39% of the total site number of the complete amino acid sequence in humans, and the 7-protein set, 76% of it. The 7-protein set did not include ND3 and ATP8 with small numbers of helices (3 or less in humans). As seen in Table 2, *TC* provided predominantly strong correlations with *HYD* in all protein sets, and the strongest correlation ($R^2 = 0.9$) in the 5-protein set (Figure 1). In addition to this, *TC-CC*, *HYD-CC* and *HYD-STC* showed appreciable correlations. Here, we used the average values of *TC* and *HYD* in each animal group, in order to describe the correlation pattern lucidly (the raw data without the averaging procedure also showed a strong correlation of $R^2 = 0.9$ (Figure S1). As a result, the *TC*-values in Aves and Eutheria with very high *BMR* were 2.5 fold larger than those of Nematoda and Platyhelminthes with very low *BMR*, and the *HYD* values of the former were decreased by about 22% compared with those of the latter. The validity of these estimations of *TC* and *HYD* was supported by speculating the *TC* and *HYD* distributions in the helix domain of the above-mentioned 4 animal groups (Figure 2).

Table 1. *HYD-TC* and *TC-CC* correlations (R^2) within respective proteins.

	ND4	ND5	ND2	CO1	CO3	ND1	ND3*	ATP8*	CYTB	ND4L*	CO2*	ATP6*	ND6*
HYD-TC	**0.89**	**0.89**	**0.87**	**0.81**	**0.78**	**0.68**	**0.68**	**0.65**	**0.60**	**0.58**	**0.57**	**0.37**	**0.03**
TC-CC	**0.60**	**0.61**	**0.64**	**0.41**	**0.49**	**0.38**	**0.32**	**0.25**	**0.26**	**0.11**	**0.29**	**0.63**	**0.42**

The * symbol denotes 2 subunits with weak correlations (ATP6 and ND6) and 4 subunits with small numbers (3 or less in humans) of helices (ND3, ATP8, ND4L, and CO2). The analysis includes the following 13 metazoan animal groups: Porifera, Cnidaria, Mollusca, Crustacea, Hexapoda, Chelicerata, Nematoda, Platyhelminthes, Echinodermata, Fishes, Amphibia, Eutheria, and Aves.

doi:10.1371/journal.pone.0098188.t001

C) Correlations between MMP variables and total site number of amino acids

We found that the total site number (*TSN*) of amino acids in a protein set steadily changes across the 13 animal groups (by 20% as a whole) and is a good index to describe the mutually contrasting evolutionary pathways of *TC* and *HYD* in metazoans (Figure 3). The *TSN* order of the animal groups (their relative *TSN*-dependence) was invariant in all protein sets (Figure S2). As a result, *TSN* strongly correlated with *TC* and *HYD*, when the deuterostomes were excluded (Table 2). Indeed, *TC* gradually decreased with decrease in *TSN* of many animal groups except for the deuterostomes (Figure 3, blue regression line), whereas *HYD* increased with a decrease in *TSN* (Figure 3, red regression line). On the other hand, *TC* and *HYD* in the deuterostome lineage presented rapidly increasing and decreasing trends with a decrease in *TSN* towards the terminal branch of Aves, clearly splitting from the 2 regression lines. This splitting pattern could be identified by looking at the *TC-HYD* relationship of Figure 1, because the non-linear regression curve **A** ($TC = 0.429 \cdot HYD^{-4.241}$ with $R^2 = 0.90$ as a whole) was decomposed into a steep slope dotted-line **B** ($TC = -65.66 \cdot HYD + 41.75$ with $R^2 = 0.92$) for the deuterostomes and a slow slope dotted-line **C** ($TC = -18.32 \cdot HYD + 14.92$ with $R^2 = 0.89$) for the other animal groups. The splitting pattern of Figure 3 became compatible with a molecular (rRNA)-based phylogeny [21], in the point that the tree starts with the root of Porifera and splits into the two lineages of Deuterostomia and Protostomia via Cnidaria. In this way, the *TC-HYD* relationship globally reflected the evolutionary pathway of metazoans.

D) Correlations between MMP variables and *mtBMR*

We examined correlations between *mtBMR* and MMP variables (*TC*, *STC*, and *HYD*) at the same mt function level, by increasing the *F* value from 1.0 (corresponding to *msBMR*) to infinity. The *mtBMR* values were estimated by extending *msBMR* in the respective animal groups (Materials and Methods). Since the data on metazoans with low *BMR* were very limited, we here applied the recent data reported by Makarieva et al. [1] and also the AnAge database for vertebrates (Table S2). We investigated the correlation between *STC* and *mtBMR* by changing the *F*-value included in this quantity 1 from 1.0 to infinity (Materials and Methods). Then we found that excluding the *M*-dependence of *mtBMR* with $F = \infty$ provides the strongest correlation (Figure S3). As a result, *mtBMR* correlated significantly with all MMP variables (*STC*, *TC*, *HYD*, and *CC*) in almost all of the protein sets, whereas *msBMR* weakly correlated with *STC* in only the 5-, 6-, and 7-protein sets. Here, *mtBMR* showed an especially strong correlation with *STC* in all protein sets (Table 2), since *STC* well describes vertebrates [16] and this analysis includes relatively many vertebrates. Figure 4A demonstrates a typical case of the 3-protein set, which shows a significant *STC-mtBMR* correlation with markedly high *mtBMR*–values in Aves and Eutheria. We here note that the *STC-msBMR* correlation was not strong with $R^2 = 0.28$.

E) Correlations of *STC* with *MLS*

The significant correlation between *STC* and *mtBMR* prompted us to examine the relationship between *STC* and *mtBMR·MLS*, because *mtBMR·MLS* corresponds to the total consumption energy per mitochondrion during the time (*MLS*) and may therefore be interpreted as a performance of the mt function. Here, *MLS* is redefined as the mean value of the individual MLSs in an animal group. By taking account of this time effect, the *STC-mtBMR·MLS* correlation ($R^2 = 0.81$) became much stronger than the *STC-*

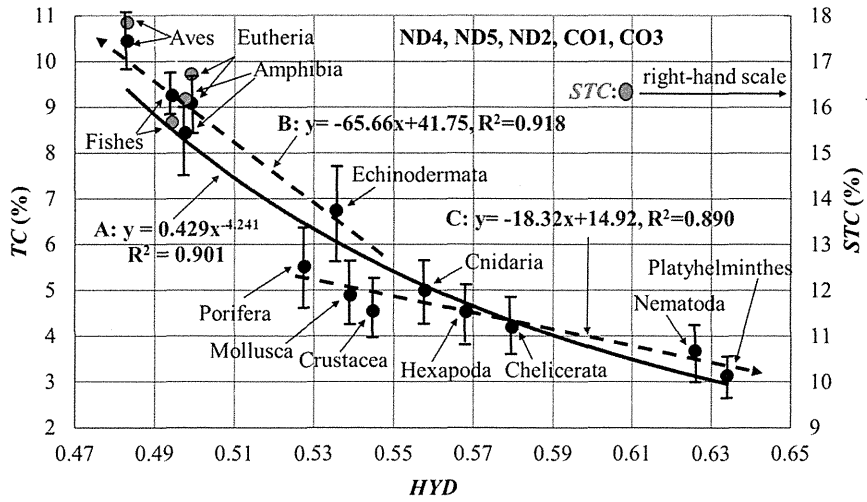

Figure 1. Global relationship between *TC* and *HYD* in MMPs of metazoan animals. Solid circles represent the average values of *HYD* and *TC* in each animal group, with the hydrophobic score S>0 (see Materials and Methods). The red circles show the *STC* values, which well describe the vertebrate lineage [16]. Such a strong correlation was also obtained by analyzing all 13 proteins (Figure S1). The correlation is totally well reproduced by a non-linear function (**A**: $TC = 0.429 \cdot HYD^{-4.2045}$ with $R^2 = 0.901$), but it can be separately expressed by 2 regression lines with different slopes (**B**: the dotted line for the deuterostomes with $R^2 = 0.918$) and (**C**: the dotted line for the other groups with $R^2 = 0.890$). The error range of the x-axis (*HYD*) in an animal group can be estimated by moving the regression curve **A** in parallel along the y-axis so that the y-value of this curve may be equal to that of the solid circle of the group, since this error range of *HYD* may be roughly given by the x-axis values of the curve corresponding to the error range of the y-axis (*STC*).
doi:10.1371/journal.pone.0098188.g001

mtBMR correlation ($R^2 = 0.64$) (the 3-protein set in Table 2), and separated vertebrates from other animal groups (Figure 4B). Figure 4C demonstrates a strong *STC-MLS* positive correlation ($R^2 = 0.71$) in the 3-protein set, and we found significant correlations between the MMP variables and *MLS* (Table 2). The *CC-MLS* correlation is likely to be related to oxidative damage to mitochondrial proteins or mtDNA [22–24], but was always weaker than the *STC-MLS* correlation in all protein sets (Table 2).

Discussion

Gradual increase in *HYD* for natural selection in many animal groups

A recent structural elucidation of ion channels in transmembrane proteins has provided evidence that these proteins undergo conformational changes during their function [13]. An easily understandable strategy of ecological and natural selection in metazoans is a reduction in their *BMR* by utilizing the multicellular effects of allometric scaling. Indeed, in many animal groups except for the deuterostomes, *HYD* and *TC* gradually

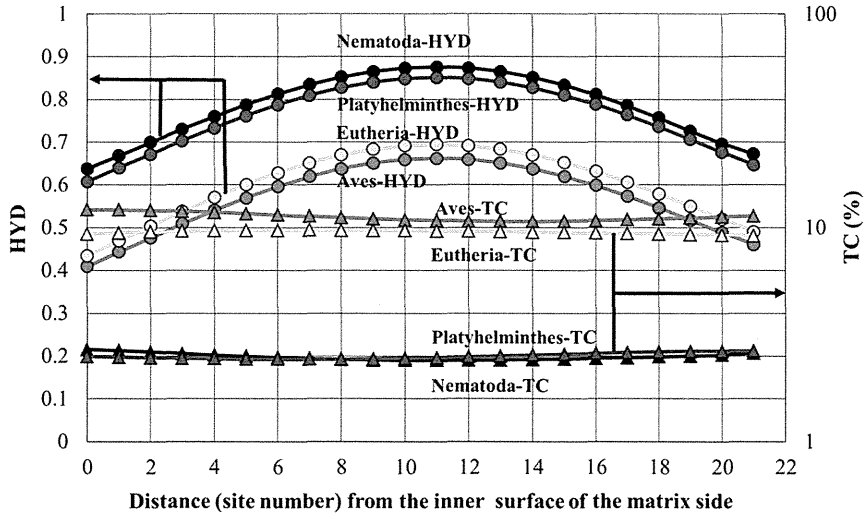

Figure 2. *HYD* and *TC* distributions in the mt inner membrane of ND2, ND4 and ND5. Four animal groups were selected as providing extreme situations of the hydrophobic distribution. This result was obtained by using SOSUI WWW server [19] and TMHMM Server [20] for the prediction of the secondary structure of proteins.
doi:10.1371/journal.pone.0098188.g002

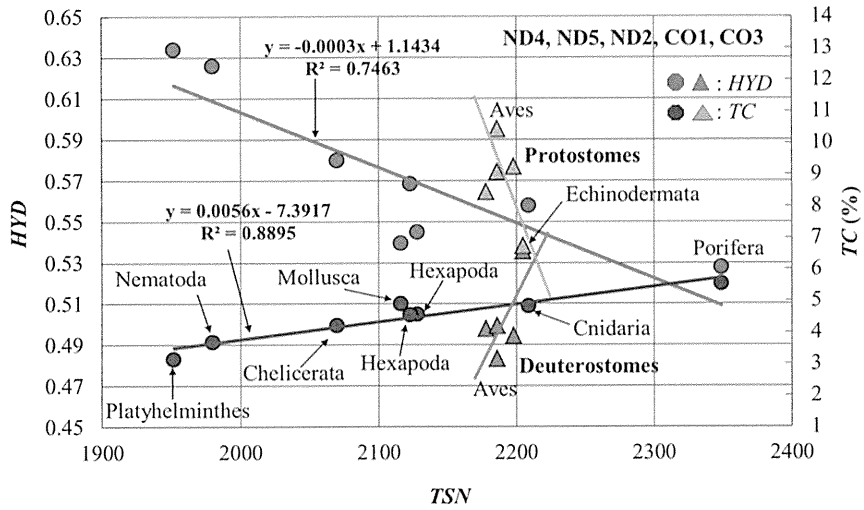

Figure 3. *HYD* and *TC* versus *TSN*. The regression lines for Deuterostomes and those for Protostomes were estimated separately. *HYD* and *TC* are expressed on the left and right ordinates, respectively.
doi:10.1371/journal.pone.0098188.g003

increased and decreased, respectively, with decrease in *TSN* (Figure 3). Here, the decrease in *TC* correlated with that in *mtBMR* (Figure 4A), since less dynamic mobility and weaker stability in MMPs balance each other for the mt function. The expression of animal groups in terms of *HYD* and *TC*/*STC* may be consistent with their phylogenetic tree. Indeed, the order of animal groups along the *TSN*-*HYD* regression line in Figure 3 became globally compatible with the branching pattern projected on the evolutional pathway from Porifera toward Platyhelminthes in the molecular (rRNA)-based phylogeny reported by Adoutte et al. [21]. This compatibility was supported by the neighbor-joining tree [25] in terms of *TSN* and *TC* (Figure S4) and also by a multidimensional vector space method of tree building (Figure S5) [26], [27]. However, the 2 lowest values of *TSN* were occupied by Platyhelminthes (Acoelomata) and Nematoda (Pseudocoelomata). The life style of these two groups seems to be closely related to each other, since they live mostly in anaerobic environments. On the other hand, the molecular-based phylogeny coupled Platyhelminthes with Mollusca (Coelomata) as Lophotropods. Apart from this problem, the gradual increase in *HYD* of MMPs well explains the evolutionary pathway of ecological selection to strengthen their stability in many animal groups except for the deuterostomes.

Increase in *STC* and decrease in *HYD* for adaptive evolution in Deuterostomes

The marked decrease in *HYD* and increase in *STC* of the deuterostome lineage are quite interesting (Figure 3), because they are likely to break the ordinary trade-off relationship rule between mobility and stability as being well understood in the evolutionary pathway of many other animal groups. These mutually reverse pathways of *HYD* and *STC* in the 2 large animal groups are far from regarding mtDNA as the neutral marker long held to be [28], cannot be explained by the nucleotide mutation pressure [29–32], and are therefore a strong evidence of adaptive evolution at the mt genome level. Another reverse process was previously observed in vertebrate marine animals such as cetaceans and alligators which returned from the land to water, because these animal groups underwent the evolutionary pathway of an increase in *HYD* and a decrease in *STC* toward Fishes in contrast to that of the decrease in *HYD* and increase in *STC* [16].

Marked decrease in *HYD* and increase in *STC* heighten mt function in vertebrates

To pursue the biological meaning of the decrease in *HYD* and increase in *STC* in the deuterostome lineage, we introduced the quantity, *mtBMR*, being an energetic function at the same mt level as *HYD* and *STC*. Indeed, *mtBMR* was correlated negatively with *HYD* and positively with *STC* (Table 2). Figure 4A demonstrates a typical *STC*-*mtBMR* correlation ($R^2 = 0.64$) in the 3-protein set (a linear combination of *STC* and *HYD* provided a stronger correlation ($R^2 = 0.77$) with *mtBMR*). The marked decrease in *HYD* supports the appearance of a very large *mtBMR* in Aves and Eutheria, since a highly active mt-function can be attained by realizing MMPs with greater conformational freedom. However, on the other hand, higher MMP instability induced by this greater freedom heightens turnover rates of mitochondria, which requires a higher cost to reproduce a large number of them within cells. Furthermore, spatial constraints in metazoan tissues make it difficult for organisms to develop much higher power by simply accumulating more mitochondria, because mitochondria in metabolically active cells (such as those of the liver and brain) of, for example, humans make up 40 percent of the cytoplasm [17]. In this situation, the marked increase in *STC* in MMPs of Aves and Eutheria must be a critical condition to compensate or overcome their instability.

The reason why Ser and Thr residues can enhance dynamic stability of MMPs

Interestingly, membrane proteins have an outstanding feature of being able to strengthen their dynamic stability by interhelical interactions between motifs involving moderately polar residues such as Ser and Thr [13–15]. Indeed, the decrease in *HYD* and increase in *STC* in Aves and Eutheria were markedly large within the membrane itself, as is well understood by comparing their differences between Aves/Eutherians and Platyhelminthes/Nematoda (Figure 2). It is therefore likely that the increase in *STC* corresponds to increased hydrogen bonding between helices, within and between subunits, as pointed out by Dawson et al. [15] and Hildebrand et al. [13]. Because Ser and Thr residues are small and only moderately polar, helical structures tend to be stabilized by cooperative networks of interhelical hydrogen bonds. In a

Table 2. Correlations (R^2) between the pairs of variables (*HYD*, *TC*, *STC*, *CC*, *TSN*, *mtBMR*, *msBMR* and *MLS*).

		3 proteins	4 proteins	5 proteins	6 proteins	7 proteins	mean
		<39%>	<47%>	<59%>	<66%>	<76%>	
TC-HYD	N	0.8898	0.8939	0.8997	0.8958	0.8867	0.89318
TC-CC	N	0.6554	0.6916	0.6994	0.7264	0.6691	0.68838
HYD-CC	P	0.5295	0.6081	0.6367	0.5449	0.5337	0.57058
HYD-STC	N	0.5052	0.4803	0.2992	0.3503	0.3151	0.3901
STC-CC	N	0.2387	0.2298	0.209	0.1887	0.1551	0.20426
TSN-TC	P	0.9232	0.9014	0.8907	0.8019	0.6699	0.83742
TSN-HYD	N	0.7591	0.7364	0.7484	0.6491	0.7171	0.7221
STC-ln(mtBMR)	P	0.6434	0.6483	0.7048	0.6762	0.6751	0.66956
TC-ln(mtBMR)	P	0.4999	0.4995	0.4948	0.5159	0.5316	0.5083
HYD-ln(mtBMR)	N	0.3403	0.3206	0.3547	0.3379	0.3574	0.34218
CC-ln(mtBMR)	N	0.4041	0.3441	0.3401	0.3184	0.2851	0.33836
STC-ln(msBMR)	P	0.1937	0.1979	0.2804	0.2514	0.2428	0.23324
STC-ln(MLS)	P	0.7065	0.6861	0.5691	0.5691	0.5687	0.6944
CC-ln(MLS)	N	0.3732	0.3962	0.3447	0.3667	0.3441	0.3654
STC-ln(mtBMR·MLS)	P	0.8133	0.8052	0.7737	0.7561	0.7551	0.78068

<n> denotes that *TSN* of each protein set occupies the n % of that of the complete amino acid sequence in Human. P and N stand for the positive and negative correlations, respectively. The best results in the respective correlation croups are denoted by italics.

doi:10.1371/journal.pone.0098188.t002

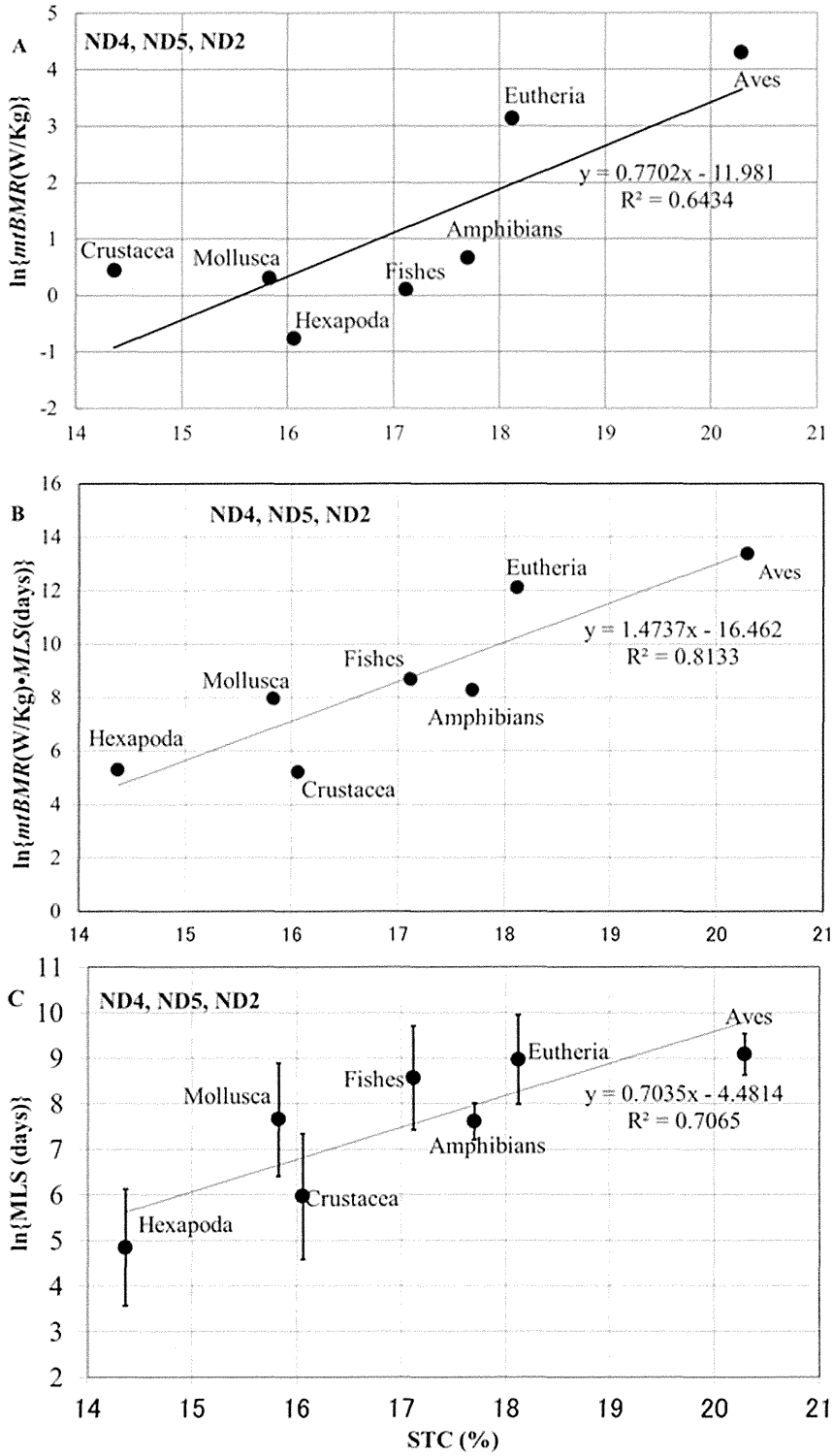

Figure 4. Relationships of *STC* with *mtBMR* (A), *mtBMR·MLS* (B), and *MLS* (C).
doi:10.1371/journal.pone.0098188.g004

previous paper [16], we showed that the short-range force of hydrogen bonds (1–2 Å) can be extended 2 to 3-fold (on average) by dynamic conformational changes in MMPs, because the relative distance of hydrogen bonding oscillates with the average amplitude R around R. Such a long-range potential amplifies the probability of interhelical interactions (in three-dimensional space) between cooperative networks of hydrogen bonds between motifs involving Thr or Ser residues. We envisage that such dynamic interactions could enable rapid resonance between metastable conformational states in MMPs, which have individual enzyme turnover rates of tens to hundreds of electrons per second [33]. In contrast, other types of hydrogen bonding, such as Cα-H---O

hydrogen bonding between Gly and Ala residues and the helical backbone, produce more rigid structures [13].

Proton-pumping machinery and dynamic conformational changes in MMPs

Three large subunits (ND2, ND4 and ND5) in complex I provided the strongest correlations between *TC* and *HYD* (Table 1), which were further correlated with *mtBMR* (Table 2). These subunits exhibit homology with sodium-proton antiporters and are known to be part of the proton pumping machinery of complex I [34]. Structural models of complex I suggest that electron transfers in the hydrophilic matrix arm are coupled to proton translocation in the membrane arm: a redox-dependent conformational change around the Q-site is transmitted to the 3 antiporter-like proton-pumping subunits (ND2, ND4 and ND5). In this way, proton translocation in complex I requires dynamic conformational changes across several subunits [4], [5], [8], [9]. Likewise, the 2 large subunits (CO1 and CO3) of complex IV, which form the second group of the strong *TC-HYD* correlations, may transfer protons across the membrane via conformational changes induced by electron transport [10], [11]. A similar relationship is also true for the proton-pumping subunits in complex III (CYTB), which is directly involved in proton-pumping via the Q-cycle. The precise mechanism of proton pumping via the Q cycle is uncertain while shuttling electrons and protons across the membrane implies a lower requirement for dynamic conformational changes in CYTB. We do indeed report a less tight correlation between *HYD* and *TC* in CYTB (Table 1). From the above-mentioned arguments, we speculate that the marked decrease in *HYD* and increase in *STC* (*TC*) in Aves and Eutheria arranged a fundamental condition to afford the powerful and robust proton-pumping machinery of complexes I and IV in these groups.

The reason why *STC* is relevant to *mtBMR* and *MLS*

The mt energy power profoundly influenced the origin and evolution of the eukaryotic cell [35], [36], and also must be closely associated with *BMR* to sustain organismal life. We noticed that variations of *mtBMR* across the different animal groups may be shielded by the very strong *M*-dependence in the allometric scaling law (as demonstrated in Mammals and Aves of Figure S6). Therefore, by defining *mtBMR* so as to minimize its *M*-dependence, we obtained a significant correlation between *mtBMR* and *STC* in contrast to a weak correlation between *msBMR* and *STC* (Table 2). The markedly large values of *mtBMR* and *STC* in Aves and Mammals strongly suggest that high degrees of dynamic conformational changes and stabilization of MMPs are realized in these animal groups, so that this stabilization effect may lower the turnover rates of mitochondria and cells, and ultimately influence organismal lifespan as well as aerobic capacity. Indeed, we obtained a significant correlation between *STC* and *MLS*, despite the enormous variations [37] in lifestyles among the different animal groups. When we recall that 10 million billion mitochondria exist in an adult human [17] and that the resources for their activation are supplied from the host cells, the stability of MMPs affecting the turnover rate of mitochondria can be a fundamental factor to sustain human life

A few animal groups of Eutheria such as rodents and insectivores (with a very high *BMR*) do not show significant *STC-HYD* and *STC-MLS* correlations [16]. These animal groups are considered to have developed a life strategy to ensure survival by countering a short longevity with quite high reproduction rates. Such behaviors in rodents and insectivores sharply contrast to those of primates with a long longevity, because a very high amino-acid replacement rate in the simian lineage is accompanied by a marked increase in *TC* and decrease in *HYD* [38]. These observations teach us that the pattern of the mt adaptive evolution is not unique even among vertebrates.

STC describes the vertebrate behavior better than TC

The potential penalties for introducing polar residues into hydrophobic membrane proteins may explain the fact that a strong inverse correlation between *HYD* and *TC* was observed across all metazoans in this study and indeed was stronger than the correlation between *HYD* and *STC*. In contrast, in our earlier studies on primates [38] and vertebrates [16], we observed strong inverse correlations between *HYD* and *STC*. The weaker correlation reported here could relate to 2 facts: the Ser residue is more polar than the Thr residue and hence is more difficult to incorporate into very hydrophobic proteins, and the hydrophobicity of MMPs is much greater in basal metazoans such as sponges and nematodes than in vertebrates. Thus it might be relatively easy to substitute Thr residues (compared with Ser) into the MMPs of basal metazoans. This interpretation is supported by the fact that substitutions of polar residues are the most common disease-causing mutations in membrane proteins, in part through altering bilayer partitioning, but also by altering function [39]. Presumably, the more hydrophobic the membrane protein, the more problems are caused by substitution of polar residues. Conversely, the less hydrophobic the protein, the less problematic is the insertion of more polar residues such as Ser. Accordingly, we note that Ser enrichment becomes more marked in the less hydrophobic MMPs of vertebrates.

Overall comments about the results

Thus, overall, our findings are consistent with the hypothesis that cooperative networks of hydrogen bonds involving Thr and Ser residues stabilize dynamic conformational changes in MMPs, presumably increasing aerobic capacity, although we have not measured that directly. Direct measurements of the effect of increased *TC* or *STC* on MMP catalytic efficiency (Kcat), either *in vitro* or *in vivo*, are very difficult, as each substitution is likely to be highly dependent on the context. Cryptic epistasis is common in molecular evolution [40], and the requirement for multiple interactions with nuclear as well as mitochondrial genes [41], [42] only makes the problem more extreme in the case of respiratory proteins. Moreover, respiratory flux can be increased by adaptations throughout the entire supply network, including lung structure, hemoglobin kinetics, and capillary density [43], [44], as well as substrate channeling via respirasome assembly [45]. Given this complexity, the pervasive correlation between *TC* (*STC*) and *HYD* in MMPs right across metazoans stands as strong evidence that selection for aerobic capacity at the level of mitochondrial-encoded subunits has indeed taken place. This view is consistent with a number of studies indicating regular selective sweeps on mitochondrial genes: mtDNA is far from the neutral marker it was long held to be [46].

Remaining problems

It was difficult to detect the species-to-species coincidence between the sequence data and the observed data on *BMR* and/or *MLS*. Therefore, we used the average values of these data in respective animal groups without taking account of this coincidence. More available data in future will provide a clearer relationship between the MMP variables and *mtBMR/MLS* in more animal groups. We did not perform temperature adjustments of metabolic rates. One reason is that a common measurement temperature does not exist because endothermic groups do not live at body temperatures of 25°C as in many other animal groups.

Another reason is that metabolic rate and temperature are not independent variables with each other, but may be rather correlated.

Conclusion

The deuterostome lineage presented a quite unique evolutionary pathway of a marked decrease in *HYD* and increase in *STC*, in sharp contrast with the pathway of many other animal groups showing a gradual increase in *HYD* and decrease in *STC*, reflecting the natural selection to utilize the multicellular effect. These decreases in *HYD* and increases in *STC* were remarkable in the 5 large subunits (ND4, ND5, ND2, CO1 and CO3) in complexes I and IV, which require their dynamic conformational changes to exert a high degree of proton-pumping function. The low *HYD* values for these subunits are congruent with the large *mtBMR* values associated with their dynamic mobility. Furthermore, the marked increase in *STC* can strengthen dynamic stability of them via helix-helix interactions. As a result, this dynamic stability can lower the turnover rate of mitochondria and cells, and ultimately prolong the lifespan of organisms. In this way, vertebrates (especially Aves and Mammals) are considered to have equipped an excellent mechanism of action in MMPs to attain both very high metabolic rate and long longevity.

Supporting Information

Figure S1 Global relationship between *TC* and *HYD* in MMPs throughout metazoans. Strong correlations with (R^2> 0.9) were obtained by analyzing all 13 proteins with S>0 (see Materials and Methods).
(TIF)

Figure S2 The *TSN*–dependence of the animal groups in various protein sets. This figure shows that the relative positions of the 13 animal groups are invariant in any protein sets of **1**) 3-protein set (ND4, ND5, ND2), **2**) 4-protein set (ND4, ND5, ND2, ND1), **3**) 5-protein set (ND4, ND5, ND2, CO1, CO3), **4**) 6-protein set (ND4, ND5, ND2, CO1, CO3, ND1), and **5**) 7-protein set (ND4, ND5, ND2, CO1, CO3, ND1, CYTB).
(TIF)

Figure S3 The *F*-value dependence of correlation (R^2) between *STC* and *mtBMR*. The correlation (R^2) between *STC* and *mtBMR* is estimated by changing the *F*-value included in this quantity from 1.0 to infinity (Materials and Methods). Here, $F=\infty$ excludes the *M*-dependence of *mtBMR* completely, and *mtBMR* depends on only the constant C in each animal group.
(TIF)

Figure S4 Neighbor-joining tree in terms of *TC* and *TSN*. We defined the pairwise distance between the i-th and j-th animal groups by $D(i, j) = \{TC(i)-TC(j)\}^{**2}/\sigma_{TC}^{**2} + \{TSN(i)-TSN(j)\}^{**2}/\sigma_{TSN}^{**2}$. $TC(i)$ and $TSN(i)$ denote the average values of *TC* and *TSN* in the i-th animal group, respectively, by using the 5-protein set (ND4, ND5, ND2, CO1, and CO3). σ_{TC} and σ_{TSN} denote the standard deviations of *TC* and *TSN*, respectively.
(TIF)

Figure S5 Two dimensional display of a tree prepared by a multidimensional vector space method. According to the multidimensional vector space (MVS) method for preparation of a phylogenetic tree [19], the molecular evolution of a tree branch is described as going into a new dimensional space, the direction of which is therefore perpendicular to that of the original pathway. For simplicity, let us consider a tree structure in 2-dimensional (X-Y) space, as illustrated in this figure. Here, the lineage **A** represents the main pathway from the tree root to species α, and the lineage B represents a branch pattern from the lineage **A** toward species β. When X and Y are variables independent from each other without any attractions (convergent evolution), the angle between the 2 lineages is 90° (when they are closely correlated, the angle may be much deviated from 90°, as seen in the case of lines **B** and **C** of Figure 1 for the *HYD-TC/STC* strong correlation). The other species except for **A**, **B** and tree root must lie on the line **A** or **B** because they evolve into new dimensional spaces. If there are long-branch attractions, they fluctuate around these lines, as seen in this figure. We note that the lineage C may include many species but degenerates into one point in the X-Y plane and that the variables (to be used) must identify as many species as possible so as to explicitly describe a tree structure within these variables.
(TIF)

Figure S6 The *M*-dependence of *BMR* in Aves and Mammals.
(TIF)

Table S1 The accession numbers of amino acid sequences of 13 animal groups.
(XLSX)

Table S2 A list of *msBMR* in the7 metazoan animal groups. The 4 quantities of *msBMR*, scaling exponent α and constant C is defined in Materials and Methods.
(XLSX)

Acknowledgments

YK is grateful to Dr. Nick Lane (University College London) for valuable discussions and insights on mitochondrial function, and thanks Drs. Junichiro Futami (Okayama University), Keiko Udaka and Takeshi Agatsuma (Kochi Medical School) for constructive discussions.

Author Contributions

Analyzed the data: YK MT. Wrote the paper: YK. Conceived the direction of research: YK MT. Read and approved the final manuscript: YK MT.

References

1. Makarieva AM, Gorshkov VG, Chown BL, Reich PB, Gavrilov VM (2008) Mean mass-specific metabolic rates are strikingly similar across life's major domains: Evidence for life's metabolic optimum. Proc Natl Acad Sci USA 105: 16994–16999.
2. Porter RK, Brand MD (1995) Causes of the difference in respiration rates from mammals of different body mass. Am J Physiol 269: R1213–R1224.
3. Porter RK (2001) Allometry of mammalian cellular oxygen consumption. Cell Mol Life 58: 815–822.
4. Mourier A, Larsson NG (2011) Tracing the trail of protons through complex I of the mitochondrial respiratory chain. PLoS Biol 9(8): e1001129. doi: 10.1371.
5. Baradaran R, Berrisford JM, Minhas GS, Sazanov LA (2013) Crystal structure of the entire respiratory complex I. Nature 28: 494(7438):443–448. doi: 10.1038.
6. Efremov RG, Baradaran R, Sazanov LA (2010) The architecture of respiratory complex I. Nature 465: 441–445.
7. NCBI genome database. Available: http://www.ncbi.nlm.nih.gov/genomes/.
8. Efremov RG, Sazanov LA (2011a) Structure of the membrane domain of respiratory complex I. Nature 476: 414–420.
9. Efremov RG, Sazanov LA (2011b) Respiratory complex I: 'steam engine' of the cell? Curr Opin Struct Biol 21: 532–540.
10. Tsukihara T, Shimokata K, Katayama Y, Shimada H, Muramoto K, et al. (2003) The low-spin heme of cytochrome c oxidase as the driving element of the proton-pumping process. Proc Natl Acad Sci USA 100: 15304–09.
11. Yamashita T, Voth GA (2012) Insights into the mechanism of proton transport in cytochrome c oxidase. J Am Chem Soc 134: 1147–1152.

12. Marechal A, Meunier B, Lee D, Orengo C, Rich PR (2012) Yeast cytochrome c oxidase: A model system to study mitochondrial forms of the haem–copper oxidase superfamily. Biochim Biophys Acta 1817: 620–628.
13. Hildebrand PW, Güther S, Goede A, Forrest L, Frömmel C, et al. (2008) Hydrogen-bonding and packing features of membrane proteins: functional implications. Biophys J 94: 1945–1953.
14. Eilers M, Shekar SC, Shieh T, Smith SO, Fleming PJ (2000) Internal packing of helical membrane proteins. Proc Natl Acad Sci USA 97: 5796–5801.
15. Dawson JP, Weinger JS, Engelman DM (2002) Motifs of serine and threonine can drive association of transmembrane helices. J Mol Biol 316: 799–805.
16. Kitazoe Y, Kishino H, Hasegawa M, Matsui A, Lane N, et al. (2011) Stability of mitochondrial membrane proteins in terrestrial vertebrates predicts aerobic capacity and longevity. Genome Biol Evol 3: 1233–1244.
17. Lane N (2005) Power, Sex, Suicide: Mitochondria and the Meaning of Life. Oxford: Oxford University Press.
18. Cowan R, Whittaker RG (1990) Hydrophobicity indices for amino acid residues as determined by high-performance liquid chromatography. Pept Res 3: 75–80.
19. SOSUI WWW server: Classification and secondary structure prediction of membrane proteins. Available: hppt://bp.nuap.nagaoya-u.ac.jp/sosui/.
20. TMHMM Server v. 2.0: Prediction of transmembrane helices in proteins. Available: http://www.cbs.dtu.dk/services/TMHMM/.
21. Adoutte A, Balavoine G, Lartillot N, Lespinet O, Prud'homme B, et al. (2000) The new animal phylogeny: Reliability and implications. Proc Natl Acad Sci USA 97: 4453–4456.
22. Moosmann B, Behl C (2008) Mitochondrially encoded cysteine predicts animal lifespan. Aging Cell 7: 32–46.
23. Schindeldecker M, Stark M, Behl C, Moosmann B (2011) Differential cysteine depletion in respiratory chain complexes enables the distinction of longevity from aerobicity. Mech Ageing Dev 132: 171–179.
24. Moosmann B (2011) Respiratory chain cysteine and methionine usage indicate a causal role for thiyl radicals in aging. Exp Gerontol 46: 164–169.
25. Saitou N, Nei M (1987) The neighbor-joining method: a new method for reconstructing phylogenetic trees. Mol Biol Evol 4: 406–425,
26. Kitazoe Y, Kurihara Y, Narita Y, Okuhara Y, Tominaga A, et al. (2001) A new theory of phylogeny inference through construction of multidimensional vector space. Mol Biol Evol. 18: 812–828.
27. Kitazoe Y, Kishino H, Okabayashi T, Watabe T, Nakajima N, et al. (2005) Multidimensional vector space representation for convergent evolution and molecular phylogeny. Mol Biol Evol 22:704–715.
28. Bazin E, Glemin S, Galtier N (2006) Population size does not influence mitochondrial genetic diversity in animals. Science 312: 570–572.
29. Reyes A, Gissi C, Pesole G, Saccone C (1998) Asymmetrical directional mutation pressure in the mitochondrial genome of mammals. Mol Biol Evol 15: 957–966.
30. Schmitz J, Ohme M, Zischler H (2002) The complete mitochondrial sequence of Tarsius bancanus: evidence for an extensive nucleotide compositional plasticity of primate mitochondrial DNA. Mol Biol Evol 19: 544–553.
31. Gibson A, Gowri-Shankar V, Higgs PG, Rattray M (2005) A comprehensive analysis of mammalian mitochondrial genome base composition and improved phylogenetic methods. Mol Biol Evol 22: 251–264.
32. Jobson RW, Dehne-Garcia A, Galtier N (2010) Apparent longevity-related adaptation of mitochondrial amino acid content is due to nucleotide compositional shifts. MITOCH. 10: 540–547.
33. Suarez RK, Staples JF, Lighton JRB (1999) Turnover rates of mitochondrial respiratory chain enzymes in flying honeybees (*Apis mellifera*). J Exp Biol 284: 1–6.
34. Mathiesen C, Hägerhäll C (2002) Transmembrane topology of the NuoL, M and N subunits of NADH:quinone oxidoreductase and their homologues among membrane-bound hydrogenases and bona fide antiporters. Biochim Biophys Acta Dec 2:121–132.
35. Lane N, Martin W (2010) The energetics of genome complexity. Nature 467: 929–934.
36. Lane N (2011a) Energetics and genetics across the prokaryote-eukaryote divide. Biol Direct 6: 35.
37. Owen RJ, Alexander S, Roberto SG, Carlo GC, Ralf S, et al. (2014) Diversity of ageing across the tree of life. Nature 505: 169–174.
38. Kitazoe Y, Kishino H, Hasegawa M, Nakajima N, Thorne JL, et al. (2008) Adaptive threonine increase in transmembrane regions of mitochondrial proteins in higher primates. PLoS One. 3: e3343.
39. Joh NHJ, Min A, Faham S, Whitelegge JP, Yang D, et al. (2008) Modest stabilization by most hydrogen-bonded side-chain interactions in membrane proteins. Nature 453: 1266–1272.
40. Lunzer M, Golding GB, Dean AM (2010) Pervasive cryptic epistasis in molecular evolution. PLoS Genet 6: e1001162.
41. Lane N (2011b) Mitonuclear match: optimizing fitness and fertility over generations drives aging within generations. BioEssays 33: 860-869.
42. Lane N (2011c) The costs of breathing. Science 334: 184–5.
43. Suarez RK (1998) Oxygen and the upper limits to animal design and performance. J Exp Biol 201: 1065–1072.
44. Maina JN (2000) What it takes to fly: the structural and functional respiratory refinements in birds and bats. J Exp Biol 203: 3045–3064.
45. Acin-Perez R, Fernández-Silva P, Peleato ML, Pérez-Martos A, Enriquez JA (2008) Respiratory active mitochondrial supercomplexes. Mol Cell 32: 529–539.
46. Bazin E, Glemin S, Galtier N (2006) Population size does not influence mitochondrial genetic diversity in animals. Science 312: 570–572.